

How complex are galaxies? A non-parametric estimation of the intrinsic dimensionality of wide-band photometric data

Corentin Cadiou,^{1,2*} Clotilde Laigle,² and Oscar Agertz¹

¹Lund Observatory, Division of Astrophysics, Department of Physics, Lund University, Box 43, SE-221 00 Lund, Sweden

²Sorbonne Université, CNRS, UMR 7095, Institut d'Astrophysique de Paris, 98 bis Boulevard Arago, F-75014 Paris, France

Accepted XXX. Received YYY; in original form ZZZ

ABSTRACT

Galaxies are complex objects, yet the number of independent parameters to describe them remains unknown. We present here a non-parametric method to estimate the intrinsic dimensionality of large datasets. We apply it to wide-band photometric data drawn from the COSMOS2020 catalogue and a comparable mock catalogue from the HORIZON-AGN simulation. Our galaxy catalogues are limited in signal-to-noise ratio in all optical and NIR bands. Our results reveal that most of the variance in the wide-band photometry of this galaxy sample can be described with at most 4.3 ± 0.5 independent parameters for star-forming galaxies and 2.9 ± 0.2 for passive ones, both in the observed and simulated catalogues. We identify one of these parameters to be noise-driven, and recover that stellar mass and redshift are two key independent parameters driving the magnitudes. Our findings support the idea that wide-band photometry does not provide more than one additional independent parameter for star-forming galaxies. Although our sample is not mass-limited and may miss some passive galaxies due to our cut in SNR, our work suggests that dimensionality reduction techniques may be effectively used to explore and analyse wide-band photometric data, provided the used latent space is at least four-dimensional.

Key words: methods: data analysis – galaxies: fundamental parameters – galaxies: formation

1 INTRODUCTION

In the past decades, we have collected exquisite multi-wavelength photometric data for millions of galaxies in the observable Universe, e.g. on COSMOS (Scoville et al. 2007) and SXDS (Mehta et al. 2018) fields, or through the HSC-SSP (Aihara et al. 2018) and DES (Hartley et al. 2022) surveys, among others. The pace of observations is now accelerating and current and next generations of space-based instruments, including JWST (Gardner et al. 2006), *Euclid* (Laureijs et al. 2011), the Vera Rubin (Ivezić et al. 2019) and the Nancy Grace Roman (Spergel et al. 2015) observatories, will provide in the next few years broad-band optical and near-infrared fluxes for almost all galaxies in the observable Universe over at least the last 10 billion years of history. These photometric datasets represent a goldmine to constrain galaxy formation, evolution and quenching from their photometry.

Galaxy photometric fluxes are directly sensitive to the complex age and metallicity distributions of the stellar population that comprise them. Traditionally, astronomers have focused on separating star-forming and passive populations based on two-dimensional colour-colour and colour-magnitude diagrams (CMDs; e.g. De Vaucouleurs 1961; Strateva et al. 2001; Bell et al. 2003; Bell et al. 2004; Arnouts et al. 2013). Recently, more sophisticated techniques have been explored to efficiently reduce dimensionality while preserving the topology of data, trying to unfold as much as possible the high-

dimensional space of galaxy colours into a single two-dimensional manifold.

For example, self-organising maps (SOMs, Kohonen 1982, 2001) are now widely used as a way to circumvent SED-fitting (see e.g. Hemmati et al. 2019). In this approach, a SOM is first built as an unsupervised classification of galaxies based on their photometric colours. In a second step, provided a representative fraction of galaxies have a label of the quantity that we want to predict, e.g. redshift, mass, star formation rate (SFR), etc., this information can be efficiently propagated to the rest of the sample. This technique was tested in simulations (e.g. Davidzon et al. 2019) and applied to observed datasets to predict redshift (Wilson et al. 2020), SFR (Davidzon et al. 2022), or redshift distribution in tomographic bins for weak lensing studies, such as DES and *Euclid* (see e.g. Buchs et al. 2019; Myles et al. 2021). As an efficient way to compare the multi-wavelength colour distribution of two galaxy samples, SOMs are also used to improve the completeness of spectroscopic sample, the representativity of which is pivotal to calibrate the photometric redshifts (e.g. the C3R2 spectroscopic calibration sample for *Euclid*, see Masters et al. 2015; *Euclid* Collaboration et al. 2022b). In addition to SOMs, other unsupervised dimensionality reduction techniques have been explored to study large datasets, such as t-SNE (Steinhardt et al. 2020), locally-linear embedding (Vanderplas & Connolly 2009) or autoencoders (Portillo et al. 2020).

Implicitly, these works assume that the manifold occupied by galaxies in photometric magnitude space can be projected in typically two dimensions without significant loss of information. While

* E-mail: corentin.cadiou@fysik.lu.se

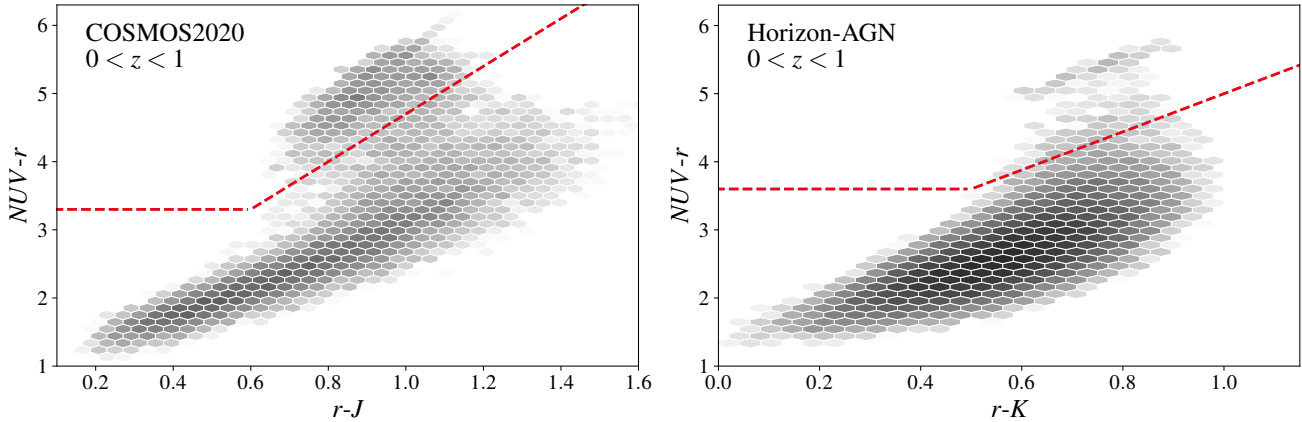


Figure 1. Colour-colour diagram used to distinguish passive from star-forming galaxies in the COSMOS2020 (*left*, $NUV - r$ versus $r - J$ rest-frame plane) and HORIZON-AGN (*right*, $NUV - r$ versus $r - K_s$ rest-frame plane) catalogues. Here we display galaxies in the redshift range $0 < z < 1$ and with mass larger than $10^{9.5} M_{\odot}$. Passive galaxies are located in the top left corner.

this implicit assumption is convenient for visualisation purposes, the choice of two dimensions isn't based on any rigorous argument. Indeed, the question of the complexity of galaxy formation is still open. Several studies have used a principal component analysis (PCA) to quantify the number of parameters needed to capture the variance in the observed properties of galaxies, with the main findings being that only a handful are required (in observations of 21cm emission, Disney et al. (2008), in SDSS spectra, Sharbaf et al. (2023)). One limitation of using PCA is however that it is a linear method, and thus cannot capture non-linear correlations between the observables, and should thus be interpreted as an upper limit on the actual dimensionality of the data. Similarly, machine learning approaches suggest that galaxies lie on a low-dimensionality manifold (Villaescusa-Navarro et al. 2022; Echeverri-Rojas et al. 2023; Chawak et al. 2023). Taken at face value, this is at odds with theory, where models of galaxy formation involve complex physical mechanisms (see e.g. Somerville & Davé 2015). Those depend, at least, on the mass of the halo, its angular momentum distribution, the impact parameter and timing of the mergers, and the non-linear physics of gas cooling, star formation, and stellar/AGN feedback processes, suggesting that galaxy formation unravels in high-dimensional parameter space.

The complexity of galaxy formation has however been recently questioned. Indeed, simulations have revealed that, at fixed galaxy mass, the scatter in properties such as disk sizes may be driven by the misalignment between the inertia tensor and tidal tensor in the initial conditions (Cadiou et al. 2022; Moon & Lee 2024), potentially explaining the origins of scatter in well-established scaling relations such as the size-magnitude relation (Courteau et al. 2007). In this picture, galaxy formation is a self-regulated process, where only a subvolume of the parameter space is accessible by the global properties of galaxies.

In this paper, we aim to answer the question of the dimensionality of the manifold occupied by galaxies in the multi-dimensional space of their photometric magnitudes. We rely on observations of hundreds of thousands of galaxies from the COSMOS catalogue, and simulated ones from the HORIZON-AGN simulation; we describe these datasets in section 2. We then present our parameter-free method, based on the approach of Granata & Carnevale (2016), to estimate their intrinsic dimensionality in section 3. We discuss our results in section 4 and wrap up in section 5.

2 CATALOGUE DATA

2.1 The COSMOS2020 catalogue

We rely on the COSMOS2020 catalogue (Weaver et al. 2022) to estimate the dimensionality of galaxy photometry. COSMOS2020 is a deep multi-wavelength catalogue extracted from the COSMOS field. It includes the photometry in 35 filters from Ultraviolet (UV) to infrared (IR). The improvement of this catalogue with previous versions is especially driven by deeper optical, NIR and IR data obtained with the HSC camera (Miyazaki et al. 2018) on the Subaru telescope, the VIRCAM instrument on the VISTA telescope (as part of the UltraVISTA survey, see McCracken et al. 2012; Euclid Collaboration et al. 2022a), and the IRAC instrument on the Spitzer telescope (as part of the SPLASH survey, see Steinhardt et al. 2014). In the following, we use the CLASSIC version of the catalogue, that is, the one that uses the photometry obtained with SEXTRACTOR (Bertin & Arnouts 1996). More specifically, galaxies were identified from a $izYJHK_s$ chi-squared image, and magnitudes are extracted in a $2''$ aperture reaching a 3σ -depth of 28.1 and 25.3 in the g -band and the K -band respectively. A full description of the catalogue preparation can be found in Weaver et al. (2022). We remove from the sample all galaxies that have been flagged as being near bright sources and areas affected by artefacts. The total area after accounting for these masks is 1.27 deg^2 . We use galaxy properties (redshifts, masses and rest-frame UVJ) derived through the LEPHARE code (Ilbert et al. 2006).

2.2 The HORIZON-AGN mock catalogue

We work with a simulated catalogue to investigate the effect of noise in the data, and to explore how different is the dimensionality of galaxy photometry when estimated either from their apparent or absolute magnitudes.

The HORIZON-AGN hydrodynamical simulation (Dubois et al. 2014), run with the adaptive mesh refinement code RAMSES (Teyssier 2002), was used to produce a mock catalogue with the same properties as the observed COSMOS2020 sample. HORIZON-AGN has a box size of $100 \text{ Mpc}/h$ and a DM mass resolution of $8 \times 10^7 M_{\odot}$. In brief, the simulation includes gas heating, cooling, star formation, feedback from stellar winds, type Ia and type II supernovae with mass, energy, and metal release in the interstellar medium,

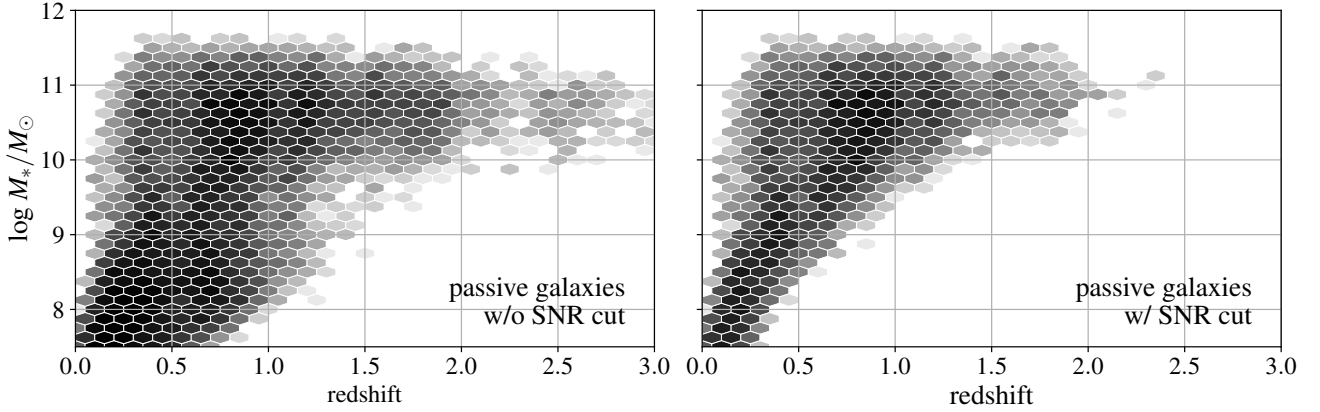


Figure 2. The mass and redshift distribution of passive galaxies in the whole sample (*left*) and after having applied the $\text{SNR} > 2$ cut (*right*). Our sample is biased towards high-mass and low redshift passive galaxies, for which significant flux may be detected in all bands.

and black hole formation. Depending on the accretion rate, AGNs release energy in a quasar or radio mode. A light cone was extracted on the fly to build realistic mocks¹ (Laigle et al. 2019; Gouin et al. 2019).

Galaxies were extracted based on the position of stellar particles using the ADAPTAHOP structure finder (Aubert et al. 2004; Tweed et al. 2009). Mock spectra were produced for each galaxy, assuming Bruzual & Charlot (2003) synthetic stellar population models and a Chabrier initial mass function (Chabrier 2003). Dust attenuation was implemented for each star particle using the gas-metal mass distribution along the line-of-sight as a proxy for the dust distribution. All details about the spectra computation can be found in Laigle et al. (2019). In addition to spectra, both absolute and apparent magnitudes were extracted in the same photometric filters as available in the COSMOS2020 catalogue. Mock photometric fluxes were perturbed by assuming a combination of Poisson noise and Gaussian noise, considering in each filter the same depth as the COSMOS2020 catalogue, so that galaxies of similar luminosity have a similar signal-to-noise ratio (SNR) in the mock and in the observed catalogues.

Overall, the galaxy populations agree well with the observations, but some discrepancies must be mentioned (Kaviraj et al. 2017). HORIZON-AGN produces galaxies that are too massive for their halo, in particular at low masses and low redshift. As a result, the stellar-to-halo mass ratio is up to 10 times larger than expected observationally in haloes of mass $10^{11} M_{\odot}$ (Shuntov et al. 2022). Furthermore, massive passive galaxies at low redshift are not as numerous as in observations, due to residual star formation in massive galaxies, and low-mass galaxies are not star-forming enough (see e.g. Dubois et al. 2016).

2.3 Dataset selection

Filter set: We estimate the dimensionality of the galaxy distribution based on the following fourteen fiducial broad-band filters: u^* , g , r , i , z , y , Y , J , H , K_s , B , V and IRAC’s CH1 and CH2. The full definition of these filters is provided in Weaver et al. (2022). Unless stated otherwise, this set of fourteen filters is the one used throughout the analysis. However, because of their width, photometry in

broad-band filters cannot easily isolate the emission by the continuum from the nebular emission lines. The latter, which could carry additional information with respect to the continuum, can be captured when adding narrow-band filters to the filter set. To that end, we also consider the fourteen narrow-band filters are also available in the COSMOS2020 catalogue in the range $[0.5, 0.8] \mu\text{m}$. We will also quantify in the following the change in dimensionality due to their addition to our fiducial filter set.

Passive galaxy identification: Passive galaxies in HORIZON-AGN were identified from their position in the $\text{NUV} - r$ versus $r - K_s$ rest-frame plane. More specifically, we define passive galaxies as those with $(\text{NUV} - r > 2.8(r - K_s) + 2.2) \ \& \ (\text{NUV} - r > 3.6)$. This empirical definition provides the best segregation between passive and star-forming galaxies in the HORIZON-AGN simulated light cone. In observations, we adopt the usual definition based on the $\text{NUV} - r$ versus $r - J$ rest-frame plane, to match previous observational works (Ilbert et al. 2013; Laigle et al. 2016; Weaver et al. 2023), with $(\text{NUV} - r > 3(r - J) + 1.2) \ \& \ (\text{NUV} - r > 3.1)$. We show the colour-colour diagrams on Fig. 1 together with our selection for the COSMOS and HORIZON-AGN datasets. We also note that the definition of passive galaxies is slightly different in the simulated and observed datasets, to account for the difference outlined in section 2.2 in terms of star-formation between the observed and simulated populations. However, the method we propose in the following provides an ensemble average of the dimensionality and is thus insensitive to where exactly the cuts are done, as long as they are sufficiently far from the bulk of the distribution.

Signal-to-noise ratio: In order to limit the impact of noise on our results, we keep only galaxies for which $\text{SNR} > 2$ in each band in each catalogue. We note that this cut will introduce a bias in the sample, since it imposes that galaxies emit flux even in the bluest bands. It therefore excludes those very passive and faint galaxies which remain undetected in the bluest bands, and limits the maximum redshift that we can probe. As an illustration, we show in Fig. 2 the distribution of passive galaxies as a function of mass and redshift with and without the SNR cut. Passive galaxies at high redshift and in the relatively low mass range are not present with the SNR cut. Similarly, very dusty star-forming galaxies are likely to be excluded from the sample with this SNR cut.

We list in Table 1 all the datasets together with the selection

¹ a version of which being publicly available at [Horizon-AGN Virtual Observatory](https://horizon-agn.github.io/).

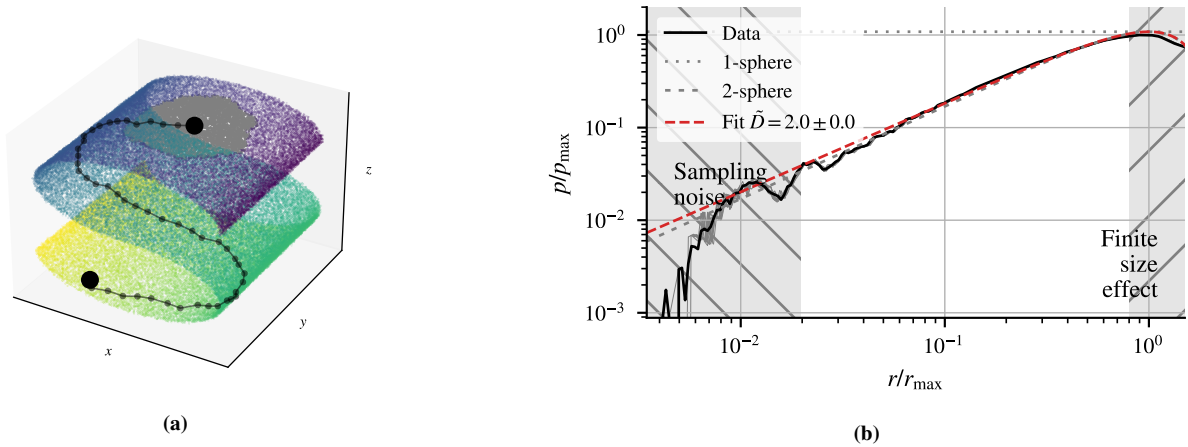


Figure 3. The dimensionality of a dataset can be estimated from the distribution of distances between points. On the left (a) the distribution of 100 000 points drawn from a 2D S-curve and embedded in 3D. The distance between two points (large black dots) can be computed by finding the shortest path between them (black dotted line, we represent one point every ten for clarity) from nearest neighbour to nearest neighbour. We show all the points within a distance r from the starting point in gray. The number of such points grows here as r^2 ; in general, it grows as r^D . By measuring the probability p of finding a point within a distance r , we can thus estimate the intrinsic dimensionality of the dataset, as is shown on the right (b). We detail the procedure in the text.

operated, along with the number of galaxies in each sample. We note that, for the sake of consistency, we use the same subset of simulated galaxies that have a $\text{SNR} > 2$, including in the datasets with no simulated noise. We checked that including galaxies with $\text{SNR} < 2$ does not change the results obtained for the mock dataset with no simulated noise, and yields consistent results for the COSMOS catalogues, albeit with larger error bars. We however note that those faint galaxies may have an intrinsically different dimensionality. We however find that, should that be case, the signal would be hidden beyond the relatively high noise level.

3 DIMENSIONALITY ESTIMATION

In this work, we aim to measure the intrinsic dimensionality D of wide-band photometric data of galaxies. Our data is comprised of N bands with a sample size of N_g galaxies. To that end, we propose to employ the method first presented in Granata & Carnevale (2016) to measure the intrinsic dimensionality.

Let us present this method qualitatively. If the distance between points in the feature space is given by the function d , let us define the probability of finding a point at separation r as

$$p(r) = \frac{2}{N(N-1)} \sum_{i < j} \delta_D(d(\mathbf{x}_i, \mathbf{x}_j) - r), \quad (1)$$

where δ_D is the Dirac delta function and \mathbf{x}_i is the data-vector of the i^{th} data point. If the manifold is compact, as is the case for photometric data, this probability eventually falls to zero as there are no points infinitely far from one another. Similarly, the probability of finding two points vanishes at small separations, unless the intrinsic dimension is null as well. Indeed, at small separations, the number of points within a distance r from a point at position \mathbf{x} goes as r^D , so $p(r)$ scales as r^{D-1} . If the distance function d is the Euclidean distance in the embedding space, Eckmann & Ruelle (1992) showed that the number of points required for accurate measurement of the intrinsic dimensionality scales as $N \sim 10^{D/2}$. This is a direct consequence of the well-known curse of dimensionality and the fact that limiting the analysis to the low-separation limit of $p(r)$ discards a large fraction of the data.

The procedure can however be improved by addressing these two issues, as was shown in Granata & Carnevale (2016). First, if the manifold is folded onto itself, as illustrated Fig. 3, $p(r)$ will display peaks at separations corresponding to the separation between the folds. This can be addressed by substituting the Euclidean distance between points with a graph distance, which is the length of the shortest path that connects them through the graph of k -nearest neighbours; we illustrate it in Fig. 3. This essentially allows to ‘unroll’ the manifold and regularises $p(r)$, which Granata & Carnevale (2016) showed to then be well approximated by the distribution of a D -dimensional hyper-sphere up to the maximum of $p(r)$. The latter has a simple closed-form expression, $p_{\text{sphere}, D}(r) \propto \sin^{D-1}(r\pi/2)$, which we can fit to the data. This estimator was shown to yield robust estimates of the dimensionality of a 20-dimensional dataset from a few thousand points.

In our case, we seek to measure the intrinsic dimensionality of data with shape (N_g, N) , where N_g is of the order of 10 000 to 100 000 and $N = 14$ wide photometric bands, which is well within the reach of the method. To that end, we first rescale the magnitudes into the range $[0, 1]$ using the same mapping for all bands, and we build a KD-Tree using the Euclidean distance in the embedded space. We then build the connectivity graph, where edges connect each data point to its k -nearest neighbours, increasing k from one until the graph is fully connected. We obtain a sample of pairwise distances by drawing randomly 200 points and by computing their distance to all others in the dataset². We split this sample of 200 estimates of $p(r)$ into ten subsamples, and we estimate the intrinsic dimensionality of each subsample as follows. For each of those, we normalise $p(r)$ by its maximum value and r by the corresponding radius. We then perform a least-square regression with the analytical expression of a D -dimensional hyper-sphere, $p_{\text{sphere}, D}(r/r_{\text{max}}) = C \sin^{D-1}(r\pi/2r_{\text{max}})$, with free parameters D and C . On the low-separation end, we remove radii that contain less than a thousand pairs to limit shot-noise. On the high-separation end, we truncate

² Ideally, one would compute the graph distance between all pairs of points, for example with the Floyd-Warshall algorithm (complexity $\mathcal{O}(N_g^3)$). This however proved to be prohibitively expensive and we instead resort to drawing the distances from a small subset of points.

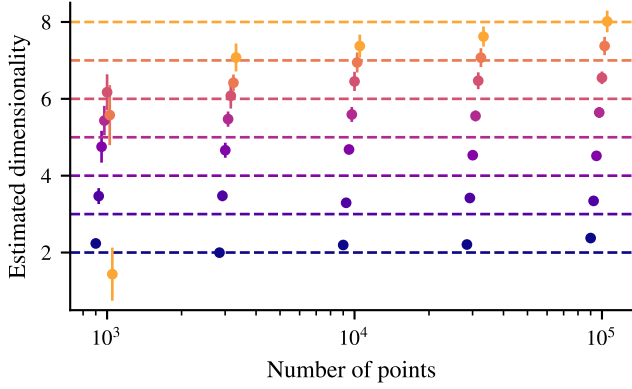


Figure 4. We use mock datasets that consist of points drawn from D -dimensional balls and measure their dimensionality as a function of the number of sample points. The ground truth values are shown as dashed lines with our estimates of the dimensionality as points with matching colour; the error bars represent the $1\text{-}\sigma$ dispersion. The accuracy of the dimensionality estimation increases with the increasing number of points. For this particular sample, our method is biased towards overestimating the actual dimensionality, but it is able to correctly distinguish datasets with an intrinsic dimensionality of up to eight.

at $r = 0.8r_{\text{max}}$ where the fit to the hyper-sphere started diverging significantly. We note that our results are robust to changes to these choices. We obtain our estimated dimensionality and its uncertainty by taking the mean and standard deviation of the ten estimates.

As an illustrative example, we show on Fig. 3, right panel, our estimate of $p(r)$ for the S-curve dataset presented in Fig. 3, left panel, sampled here with 100 000 points and embedded in 3D. We recover here an excellent agreement between the measured dimensionality and the truth value, 2. To assess the accuracy of our method, we then draw 100 000 points from a D -dimensional ball embedded in a N -dimensional space. We chose here $N = 14$ and vary D from 1 to 8. In practice, we uniformly draw points within a D -dimensional unit ball and fill the remaining dimensions with a small (10^{-2}) uniformly distributed value to mimic the effect of a small signal-to-noise. Fig. 4 shows the estimated dimensionality together with the truth value as a dashed line. We see that the accuracy of the measurement depends on the intrinsic dimensionality, with the most accurate measurements obtained for low-dimensional datasets, and on the number of points used to estimate it. We also note that our estimator is biased towards an overestimation of the actual intrinsic dimensionality by up to 0.5. While the bias may depend on the exact geometry of the manifold, we however note that, for a fixed geometry, our estimator can correctly distinguish datasets with different dimensionality. In practical terms, with a sample size of 100 000 points, we can distinguish datasets with up to seven intrinsic dimensions within one standard deviation. With a sample size of 10 000, we can distinguish datasets with up to six intrinsic dimensions.

In the following, we will mostly focus on the variation of the measured dimensionality, so that we limit the extent to which the bias is the estimator contaminates our conclusions.

4 RESULTS

First, let us compare the observed and simulated catalogues. We measure their dimensionality and present the results on Fig. 5, with data

including all galaxies from COSMOS (top) and the HORIZON-AGN mock catalogue (bottom). In both cases, we find that the dimensionality is around 4.2. Despite data from the simulation missing passive galaxies at the high-mass end and star-forming ones at the low-mass end, we, however, find that the simulated and the observed catalogues have overall similar dimensionality. To confirm that this dimensionality is driven by actual correlations in the dataset rather than an effect of the limited size of our sample, we randomly reshuffle the entries of the COSMOS datasets independently for each column to erase possible correlations. Doing so, we find a much larger dimensionality of 9.2 ± 1.2 . We however recall that such, for such high dimensionalities, our method starts saturating and this value should thus be interpreted as a lower bound on the actual intrinsic dimensionality of the data. However, this confirms that the measured dimensionality in the fiducial, unshuffled, dataset reflects internal structures rather than be an artefact of the limited size of our sample.

With this in mind, we then use the noise-free magnitudes to estimate the impact noise has on the apparent complexity of the observations. Our finding is that noise masquerades an intrinsic dimensionality of the dataset, so removing noise decreases the overall dimensionality by one (to 3.2 ± 0.1), and this despite having limited ourselves to galaxies with a signal-to-noise ratio larger than 2. The simulated dataset also allows us to employ absolute, rather than apparent, magnitudes. This removes the effect of redshift from the data. Working with noise-free apparent magnitudes, we observe that the dimensionality further decreases by one (to 2.2 ± 0.1). We interpret this as the (unsurprising) fact that one key variable driving the magnitudes in different bands is the redshift of the galaxy.

To gain further insight into the dataset, let us now split the galaxies between star-forming and passive ones, as described in section 2.3. Doing so, we find that passive galaxies have a dimensionality of 2.8 ± 0.1 (2.9 ± 0.2 in the simulated dataset), while star-forming galaxies have 4.6 ± 0.2 (4.5 ± 0.3 in the simulated dataset).

We then include in our datasets the 14 narrow-band filters, with the expectation those would encode independent information about the star-formation activity of the galaxies. We however find that the addition of those filters does not change significantly the estimate of the intrinsic dimensionality which goes from 4.2 ± 0.4 to 4.5 ± 0.3 when including the narrow-band filters. We reach a similar conclusion for star-forming galaxies (from 4.6 ± 0.2 to 4.6 ± 0.3) or passive ones (from 2.8 ± 0.1 to 2.8 ± 0.2).

Finally, we also apply our estimator to spectra in the mock catalogue, finding a dimensionality of 5.0 ± 0.3 . We warn that a careful analysis of the performance of our method should be carried out in the limit of large embedding dimensions (here, 2000) to be able to reach definitive conclusions. Notwithstanding, the measured dimensionality here is larger than the corresponding dimensionality of the wide-band photometric dataset (which is 3.2 ± 0.1). We interpret this as evidence that spectra are more information-rich and that at least two additional parameters may be extracted from them. We delay further exploration of spectra to the future.

5 CONCLUSION AND DISCUSSION

The goal of this paper was to estimate the dimensionality of broad-band photometric data. To that end, we have adapted the dimensionality-measurement technique of Granata & Carnevale (2016). Our main results are the following:

- (i) The intrinsic large-scale dimensionality of observed broad-band data is between four and five. Mocks are consistent with observations when similar level of noise and cut are applied.

Table 1. Measure of intrinsic dimensionality (ID). Here we only use high signal-to-noise ratio data. Contributions to ID: (1) measurement noise, (2) stellar mass, (3) redshift. For star-forming (SF) galaxies, an extra parameter is (4) the sSFR.

Dataset	Comment	Selection	Size	Dimensionality	Figure
HAGN		-	715 006	4.3 ± 0.2	5
		star-forming	706 720	4.5 ± 0.3	
		passive	8286	2.9 ± 0.2	
	no noise*	-	715 006	3.3 ± 0.1	
	no noise*	star-forming	706 720	3.3 ± 0.1	A3
	no noise*	passive	8286	2.2 ± 0.3	A3
	no noise*	$10.0 \leq \log_{10}(M_{\star}/M_{\odot}) \leq 10.5$	105 296	2.3 ± 0.1	
	$10.5 \leq \log_{10}(M_{\star}/M_{\odot}) \leq 11.0$	28 300	2.4 ± 0.1		
	no noise, absolute magnitudes*	-	715 006	2.2 ± 0.1	
COSMOS		-	393 118	4.3 ± 0.2	5
		star-forming	359 159	4.6 ± 0.2	A1
		passive	30 260	2.8 ± 0.1	A1
		$10.0 \leq \log_{10}(M_{\star}/M_{\odot}) \leq 10.5$	32 190	3.0 ± 0.2	
		$10.5 \leq \log_{10}(M_{\star}/M_{\odot}) \leq 11.0$	15 581	3.2 ± 0.2	

* For consistency, we select the simulated galaxies that have a large signal-to-noise in the catalogue with simulated noise.

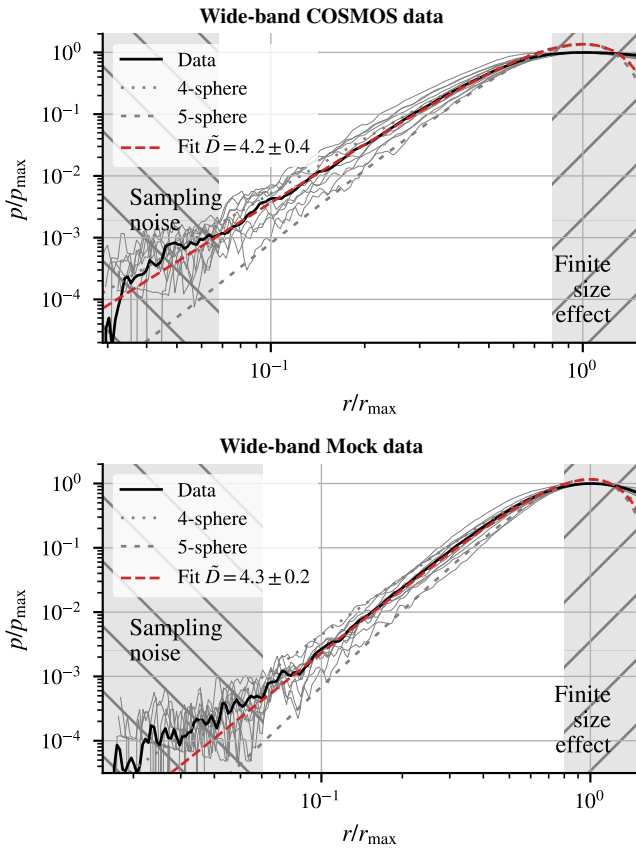


Figure 5. Wide-band photometric data from the COSMOS catalogue have a low dimensionality and are intrinsically four-dimensional. We measure the pairwise distance probability p as a function of separation r and compare it to the analytical formula of a D -dimensional hypersphere. We show in dashed red the result of the best fit. Both simulated and observed data have an intrinsic dimensionality between four and five.

(ii) Realistic estimates of the noise in the mock catalogue account for one of these dimensions.

(iii) Star-forming galaxies are intrinsically more complex ($D \sim 3 - 4$) than passive galaxies ($D \sim 2 - 3$).

Our results highlight that most of the variance in global, large-scale properties of galaxies can be described with a small number of independent parameters. This is in line with similar findings of Villaescusa-Navarro et al. (2022); Chawak et al. (2023). These previous studies relied on the use of machine-learning and focused on physical parameters (masses, radii, velocities) rather than observational ones. Our method aims at providing the number of ‘main’ parameters driving scaling relations, which we showed here to be consistent with mass, redshift, and star formation rate. In the future, we suggest extending the mock dataset to mix observational information with physical quantities, such as mass, radius, or spin. Any increase in the measured dimensionality would then suggest that the physical quantities cannot be derived from the observational ones alone. We delay such analysis to future work, as this would require carefully rescaling physical and observational parameters to allow building a similarity metric between them.

We emphasize that relatively small deviations from scaling relations are only revealed once the driving effect of these main parameters is removed. For example, when we bin by stellar mass in the noise-free absolute-magnitude simulated dataset, we find that this does not result in a decrease in the number of dimensions. Indeed, once the main parameters driving the absolute magnitudes were fixed, we started probing secondary parameters that drive the scatter around scaling relations, such that the dimensionality measurement is now probing smaller variations in magnitudes.

The exact dimensionality revealed here provides guiding numbers to employ dimensionality-reducing techniques, such as self-organised maps (Davidzon et al. 2019, 2022), locally-linear embedding (Vanderplas & Connolly 2009) or variational auto-encoders (Portillo et al. 2020). Indeed, the latent space should have at least four to five dimensions to ensure the projection doesn’t lose information.

Our results support an emerging scenario in which the main global galaxy properties evolve towards a low-dimensional attractor. This was first suggested by Disney et al. (2008), although our findings support more complexity than the one-dimensional attractor they reported. We however note that our datasets rely on photometry – and thus are affected by redshift – while theirs did not. In addition, they excluded colour information, and thus information about star-formation rate, from their analysis, while we found this information to be relevant in driving the dimensionality up.

This idea that galaxies are governed by a small number of parameters has found renewed interest with recent research suggesting that

one previously unknown key parameter driving galaxy properties is the misalignment between the inertia tensor and the tidal tensor in the initial conditions, τ . This parameter correlates well with properties in the evolved Universe such as spin and formation time (Moon & Lee 2024) or the morphology and angular momentum support of galaxies at high-redshift (Park et al. 2022). In Cadiou et al. (2022), it was additionally shown to be a cause-and-effect relationship, with higher values of the misalignment yielding less bulgy and more disk, more extended galaxies at fixed halo and stellar masses. This provides four independent parameters – (halo) mass, local density, gravitational shear (q , see e.g. Paranjape et al. 2018) and tidal misalignment (τ) – that have been shown to correlate with galaxy properties. Remarkably, this number of independent parameters is consistent with the number of dimensions we obtained from photometric surveys.

This raises the wider question of whether this set of four parameters is enough to build a complete theory capable of fully predicting the wide-band photometric survey. While this goes beyond the scope of this paper, we note that large cosmological volume simulations are finally ripe to tackle this problem from a statistical standpoint, as we did in this paper. In parallel, genetic modifications of the initial conditions (Rey & Pontzen 2018; Stopyra et al. 2021; Cadiou et al. 2021a,b; Rey et al. 2023), offer avenues to confirm the causal relation between those parameters and observables.

ACKNOWLEDGEMENTS

C.C. and O.A. acknowledge support from the Knut and Alice Wallenberg Foundation, the Swedish Research Council (grant 2019-04659), and the Swedish National Space Agency (SNSA Dnr 2023-00164). C.L. acknowledges funding from the PNCG and the French Agence Nationale de la Recherche for the project iMAGE (grant ANR-22-CE31-0007). This work has made use of the CANDIDE computer system at the IAP supported by grants from the PNCG, CNES, and the DIM-ACAV, as well as the Infinity Cluster, both hosted by Institut d’Astrophysique de Paris. We thank Stéphane Rouberol for running them smoothly for us. The authors thank C. Pichon, M. Rey, A. Glielmo and O. Ilbert for fruitful discussions. This research was supported in part by grant NSF PHY-1748958 to the Kavli Institute for Theoretical Physics (KITP).

This project has used GNU PARALLEL (Tange 2018), JUPYTER notebooks (Kluyver et al. 2016), MATPLOTLIB (Hunter 2007), NETWORKX (Hagberg et al. 2008), NUMPY (Harris et al. 2020), SCIPY (Virtanen et al. 2020) and ASTROPY³ a community-developed core Python package and an ecosystem of tools and resources for astronomy (Astropy Collaboration et al. 2013, 2018, 2022).

DATA AVAILABILITY

The data underlying this article will be shared on reasonable request to the corresponding author.

REFERENCES

Aihara H., et al., 2018, *PASJ*, 70, S4
 Arnouts S., et al., 2013, *A&A*, 558, A67
 Astropy Collaboration et al., 2013, *A&A*, 558, A33
 Astropy Collaboration et al., 2018, *AJ*, 156, 123

Astropy Collaboration et al., 2022, *ApJ*, 935, 167
 Aubert D., Pichon C., Colombi S., 2004, *MNRAS*, 352, 376
 Bell E. F., McIntosh D. H., Katz N., Weinberg M. D., 2003, *ApJS*, 149, 289
 Bell E. F., et al., 2004, *ApJ*, 608, 752
 Bertin E., Arnouts S., 1996, *A&AS*, 117, 393
 Bruzual G., Charlot S., 2003, *MNRAS*, 344, 1000
 Buchs R., et al., 2019, *MNRAS*, 489, 820
 Cadiou C., Pontzen A., Peiris H. V., 2021a, *MNRAS*, 502, 5480
 Cadiou C., Pontzen A., Peiris H. V., Lucie-Smith L., 2021b, *MNRAS*, 508, 1189
 Cadiou C., Pontzen A., Peiris H. V., 2022, *MNRAS*, 517, 3459
 Chabrier G., 2003, *PASP*, 115, 763
 Chawak C., Villaescusa-Navarro F., Rojas N. E., Ni Y., Hahn C., Angles-Alcazar D., 2023, *Cosmology with Multiple Galaxies* (arxiv:2309.12048)
 Courteau S., Dutton A. A., van den Bosch F. C., MacArthur L. A., Dekel A., McIntosh D. H., Dale D. A., 2007, *ApJ*, 671, 203
 Davidzon I., et al., 2019, *MNRAS*, 489, 4817
 Davidzon I., et al., 2022, *A&A*, 665, A34
 Disney M. J., Romano J. D., Garcia-Appadoo D. A., West A. A., Dalcanton J. J., Cortese L., 2008, *Nature*, 455, 1082
 Dubois Y., et al., 2014, *MNRAS*, 444, 1453
 Dubois Y., Peirani S., Pichon C., Devriendt J., Gavazzi R., Welker C., Volonteri M., 2016, *MNRAS*, 463, 3948
 Echeverri-Rojas N., et al., 2023, *ApJ*, 954, 125
 Eckmann J.-P., Ruelle D., 1992, *Physica D: Nonlinear Phenomena*, 56, 185
 Euclid Collaboration et al., 2022a, *A&A*, 658, A126
 Euclid Collaboration et al., 2022b, *A&A*, 664, A196
 Gardner J. P., et al., 2006, *Space Sci. Rev.*, 123, 485
 Gouin C., et al., 2019, *A&A*, 626, A72
 Granata D., Carnevale V., 2016, *Scientific Reports*, 6, 31377
 Hagberg A. A., Schult D. A., Swart P. J., 2008, in Varoquaux G., Vaught T., Millman J., eds, *Proceedings of the 7th Python in Science Conference*. Pasadena, CA USA, pp 11–15
 Harris C. R., et al., 2020, *Nature*, 585, 357
 Hartley W. G., et al., 2022, *MNRAS*, 509, 3547
 Hemmati S., et al., 2019, *ApJ*, 881, L14
 Hunter J. D., 2007, *Computing in Science Engineering*, 9, 90
 Ilbert O., et al., 2006, *A&A*, 457, 841
 Ilbert O., et al., 2013, *A&A*, 556, A55
 Ivezić Ž., et al., 2019, *ApJ*, 873, 111
 Kaviraj S., et al., 2017, *MNRAS*, 467, 4739
 Kluyver T., et al., 2016, in Loizides F., Schmidt B., eds, *20th International Conference on Electronic Publishing* (01/01/16). IOS Press, pp 87–90, doi:10.3233/978-1-61499-649-1-87
 Kohonen T., 1982, *Biological Cybernetics*, 43, 59
 Kohonen T., 2001, *Self-Organizing Maps*. Springer Series in Information Sciences Vol. 30, Springer, Berlin, Heidelberg, doi:10.1007/978-3-642-56927-2
 Laigle C., et al., 2016, *ApJS*, 224, 24
 Laigle C., et al., 2019, *MNRAS*, 486, 5104
 Laureijs R., et al., 2011, *arXiv e-prints*, p. arXiv:1110.3193
 Masters D., et al., 2015, *ApJ*, 813, 53
 McCracken H. J., et al., 2012, *A&A*, 544, A156
 Mehta V., et al., 2018, *ApJS*, 235, 36
 Miyazaki S., et al., 2018, *PASJ*, 70, S1
 Moon J.-S., Lee J., 2024, *Mutual Information between the Galaxy Properties and Initial Predisposition* (arxiv:2311.03632), doi:10.48550/arXiv.2311.03632
 Myles J., et al., 2021, *MNRAS*, 505, 4249
 Paranjape A., Hahn O., Sheth R. K., 2018, *MNRAS*, 476, 3631
 Park C., et al., 2022, arXiv:2202.11925 [astro-ph]
 Portillo S. K. N., Parejko J. K., Vergara J. R., Connolly A. J., 2020, *AJ*, 160, 45
 Rey M. P., Pontzen A., 2018, *MNRAS*, 474, 45
 Rey M. P., et al., 2023, *MNRAS*, 521, 995
 Scoville N., et al., 2007, *ApJS*, 172, 1
 Sharbaf Z., Ferreras I., Lahav O., 2023, *MNRAS*
 Shuntov M., et al., 2022, *A&A*, 664, A61

³ <http://www.astropy.org>

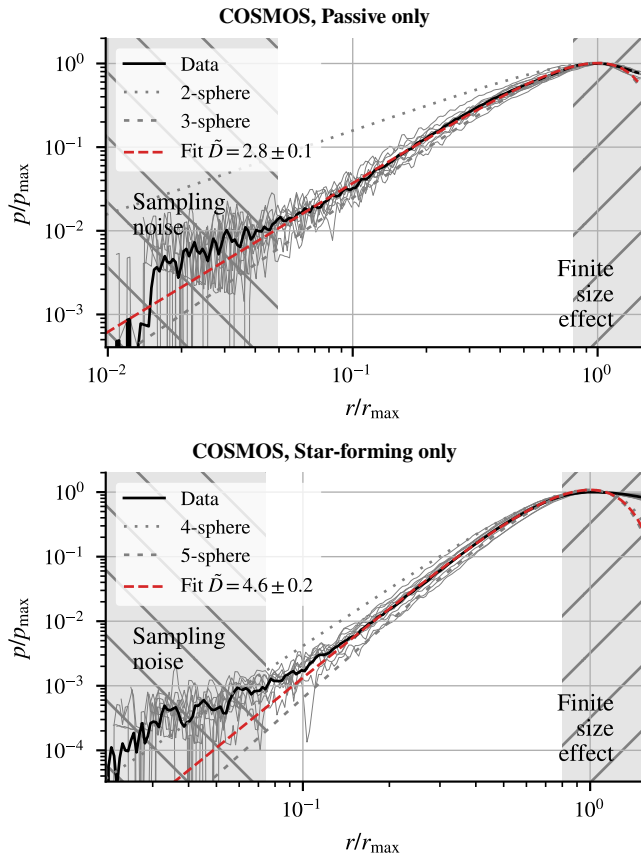


Figure A1. Same as Fig. 5, but comparing the COSMOS data with only passive (top) and only star-forming (bottom) galaxies. Star-forming galaxies have a higher intrinsic dimensionality than passive galaxies.

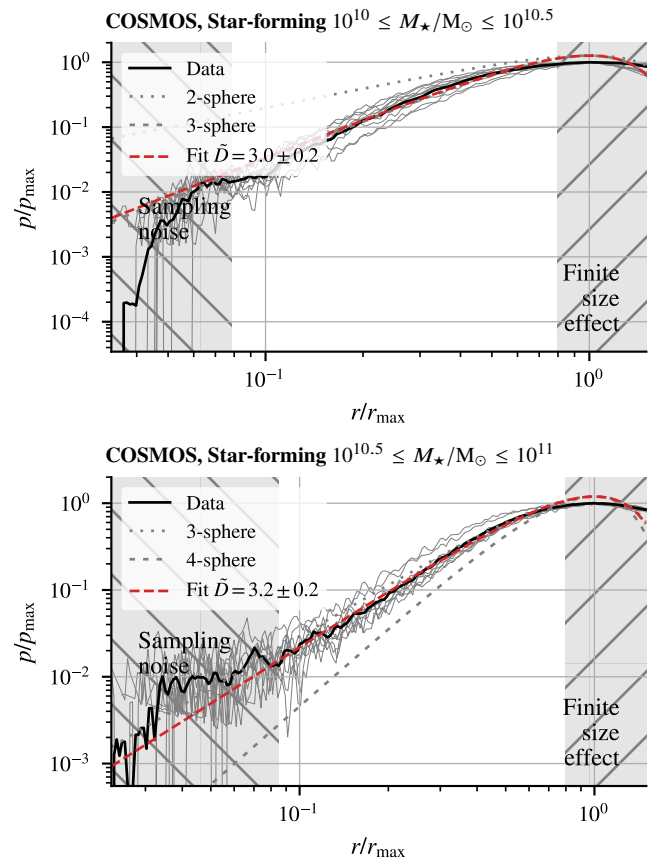


Figure A2. Same as Fig. 5, but comparing the COSMOS data with only star-forming galaxies in two mass bins. Selecting galaxies within a narrow mass range decreases the intrinsic dimensionality by one.

- Somerville R. S., Davé R., 2015, *ARA&A*, 53, 51
 Spergel D., et al., 2015, *arXiv e-prints*, p. [arXiv:1503.03757](https://arxiv.org/abs/1503.03757)
 Steinhardt C. L., et al., 2014, *ApJ*, 791, L25
 Steinhardt C. L., Weaver J. R., Maxfield J., Davidzon I., Faisst A. L., Masters D., Schemel M., Toft S., 2020, *ApJ*, 891, 136
 Stopyra S., Pontzen A., Peiris H., Roth N., Rey M. P., 2021, *ApJS*, 252, 28
 Strateva I., et al., 2001, *AJ*, 122, 1861
 Tange O., 2018, GNU Parallel 2018. Ole Tange, [doi:10.5281/zenodo.1146014](https://doi.org/10.5281/zenodo.1146014)
 Teyssier R., 2002, *A&A*, 385, 337
 Tweed D., Devriendt J., Blaizot J., Colombi S., Slyz A., 2009, *A&A*, 506, 647
 Vanderplas J., Connolly A., 2009, *AJ*, 138, 1365
 de Vaucouleurs G., 1961, *ApJS*, 5, 233
 Villaescusa-Navarro F., et al., 2022, *ApJ*, 929, 132
 Virtanen P., et al., 2020, *Nature Methods*, 17, 261
 Weaver J. R., et al., 2022, *ApJS*, 258, 11
 Weaver J. R., et al., 2023, *A&A*, 677, A184
 Wilson D., Nayyeri H., Cooray A., Häußler B., 2020, *ApJ*, 888, 83

APPENDIX A: DIFFERENT CUTS

In this section, we provide the plots corresponding to the data in Table 1.

We show on Fig. A3 the dimensionality of the mock datasets including only passive galaxies (top) and only star-forming galaxies (bottom). We find that star-forming galaxies cover a region of the parameter space with higher dimensionality.

This paper has been typeset from a \LaTeX file prepared by the author.

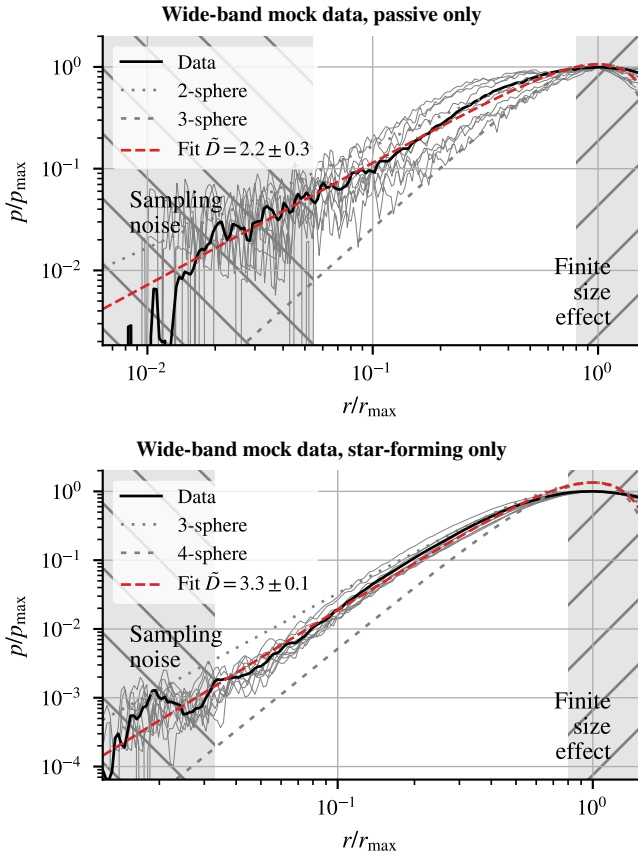


Figure A3. Same as Fig. 5, but comparing the mock data with only passive (top) and only star-forming (bottom) galaxies. Star-forming galaxies have a higher intrinsic dimensionality than passive galaxies.